Bull. Mater. Sci. (2021) 44:116
https://doi.org/10.1007/s12034-021-02422-5

Effect of Cu and N co-doping in ZnO crystals through thermal processing on energy-level distribution

LEO CHAU-KUANG LIAU* and YU-BIN HUANG
Department of Chemical Engineering and Materials Science, Yuan Ze University, Taoyuan City 32003, Taiwan
*Author for correspondence (lckliau@saturn.yzu.edu.tw)

MS received 12 November 2020; accepted 14 January 2021

Abstract. Metal- and nonmetal-doped ZnO samples, such as N-doped ZnO (NZO), Cu-doped ZnO (CZO) and Cu and N co-doped ZnO (CNZO) crystals, were synthesized and analysed. These ZnO samples were prepared by mixing precursors, such as zinc acetate, ammonia (A), ammonium acetate (AA) and copper acetate, at various proportions through thermal treatment. Results showed that the morphology, crystalline size and light absorption of the Cu- and N-doped ZnO samples were affected by different dopants. The bandgap energy (E_g) of the doped ZnO was determined and became narrow, which was attributed to the presence of N and Cu dopants using UV–vis spectral analysis. The energy bands, including the conduction band minimum (E_c) and valence band maximum (E_v), of the doped ZnO were determined using linear sweep voltammetry and UV–vis data analysis. Both E_c and E_v values for CNZO reduced in the presence of Cu and N in ZnO. The degree of energy-level variations among the doped ZnO samples was discussed and explained according to the experimental analysis.

Keywords. Cu and N co-doped ZnO; bandgap energy; energy band variation; thermal processing.

1. Introduction

The modification of zinc oxide (ZnO) to improve its material properties, such as optical, electronic and opto-electronic properties, is a crucial topic of research. Metal and nonmetal doping in ZnO are taken as effective methods to modify ZnO properties. Various doped ZnO materials have been fabricated and applied in many modern opto-electronic devices, such as photo-catalysts [1–3], water splitting [4], thin-film transistors (TFTs) [5] and light emitting diodes [6]. Studies have revealed that the device performance can be effectively improved through modification.

Metal doping in ZnO has been widely studied in recent years [1–3]. Group III elements, such as Al, Ga and In, are conductive for ZnO doping. Al-doped ZnO (AZO) transparent film has been studied using sputtering or sol–gel synthesis methods. Modified ZnO has been applied in semiconductor devices to improve the electrical conducting properties. Nomura *et al* [7] has studied In and Ga co-doped ZnO (IGZO), which has been successfully applied for fabricating TFTs through low-temperature sputtering. Stable electrical properties, e.g., charge mobility, of IGZO films can enhance TFT device performance and operation. Transition metals, such as Fe, Mn, Ni and Cu, are popular dopants for ZnO [1–3]. The light absorption of metal-doped ZnO can shift from the UV to visible region. The energy bands of various metal-doped ZnO differ in the presence of metal elements in ZnO. Cu-doped ZnO (CZO) crystals exhibit excellent structural stability, because the atomic radius of Cu is close to Zn. Thus, Cu can easily substitute Zn in ZnO crystals. The photonic bandgap energy decreased and electronic properties of CZO depend on the amount of Cu added in our previous study [8]. Although excess Cu in CZO can be used as a recombination centre, Cu-doped ZnO exhibits high O 1s binding energy and hydroxyl group content, which can suppress electron–hole recombination [9].

P [10], S [11] and N [12–25] are popular elements in nonmetal doping of ZnO. N doping in ZnO has received considerable attention among researchers because the size of the N atom is compatible to that of the O atom and the N atom has the smallest ionization energy. N-doped ZnO (NZO) was discussed by many researchers and applied in several applications, such as photocatalyst [15–23]. The photocatalytic activity of NZO can be improved in visible-light region because NZO exhibits low bandgap energy and electron–hole recombination. The NZO semiconductor changes ZnO from n-type to p-type because of the presence of N in ZnO. Several methods, including ion implantation [26] and thermal treatment [12–25], have been implemented to fabricate NZO. Among these, thermal treatment method is a popular method of NZO fabrication. In this method, NZO was prepared by passing N_2 or NH_3 gas through ZnO

Published online: 28 April 2021

during high temperature annealing. However, NZO preparation using this strategy is time-consuming and requires processing in high temperature. The other approach for NZO preparation involves the addition of N-containing additives in a Zn^{2+} solution at low temperature treatment. Common N-containing additives, such as urea [14–20], ammonia (A) [23], ammonium acetate (AA) [12,13], melamine [22] and triethanolamine [24], were used to synthesize NZO effectively after thermal processing.

Although metal- and nonmetal-doped ZnO have unique properties, metal and nonmetal co-doped ZnO has been studied to modify the optical and electrical properties of ZnO [20,27–29]. For example, AZO (Al-doped ZnO) and NZO (N-doped ZnO) exhibit different properties and have been applied to develop AZO/NZO homojunction photodiodes [24]. Al- and N-doped ZnO exhibited particular optoelectronic properties. The optical and electrical properties of the co-doped ZnO were modified by co-doping both Al and N in ZnO to improve system performance. Such co-doped ZnO was applied in photocatalytic and water splitting systems. Moreover, Co and N co-doped ZnO was fabricated for enhancing the efficiency of a water splitting system [30]. However, the influence of energy levels on the properties of metal and nonmetal co-doped ZnO has not been reported. Limited experimental studies have been conducted on Cu and N doping in ZnO (CNZO). The properties of CNZO and its potential application in optoelectronic application are yet to be analysed.

In this study, the influence of Cu and N doping in ZnO on the properties of resultant ZnO was investigated. Sources of N and metal ion additives in the precursor solutions were prepared at various ratios to fabricate the doped ZnO samples. The material properties of the prepared NZO and CNZO samples were analysed to determine the influence of Cu and N doping in ZnO. The energy band distribution of the doped ZnO was determined to demonstrate the variation in the energy levels for the doped ZnO samples. The energy-level variations of N and Cu doping in ZnO were analysed to explain the effects of the presence of the metal (Cu) and nonmetal (N) on the properties of the ZnO crystal.

2. Experimental

The ZnO and doped ZnO particles were prepared by mixing precursor at various proportions through thermal treatment. The precursor solution for ZnO was produced by preparation of 0.1 M $Zn(CH_3COO)_2$ solution at room temperature. The ZnO sample was obtained by heating the prepared solution by setting a heating rate at 2°C min^{-1} from 25 to 400°C. N-doped ZnO (NZO) samples were prepared by adding N-containing materials. Two types of nitrogen species additives, namely ammonia (A), and ammonium acetate (AA), were added in the precursor solutions to prepare the N-doped ZnO (NZO) samples. The first type of the NZO sample was prepared from the addition of 10% ammonium acetate (CH_3COONH_4) in 0.1 M $Zn(CH_3COO)_2$ solution (NZO-AA). The other type of NZO was produced by mixing 0.1 M $Zn(CH_3COO)_2$ solution and adjusting the solution to pH = 9.0 by adding 1 M $NH_{3(aq)}$ in the solution (NZO-A). The samples were heated by setting a heating rate at 2°C min^{-1} from 25 to 400°C.

The Cu-doped ZnO (CZO) precursor solution was prepared by adding 5 mol% $Cu(CH_3COO)_2$ into 0.1 M $Zn(CH_3COO)_2$ solution, which was thoroughly stirred at room temperature for 5 min. The solution was heated by setting a heating rate at 2°C min^{-1} from 25 to 400°C to fabricate CZO. Two types of Cu and N co-doped ZnO (CNZO) were prepared in this study. The first type of CNZO was prepared from the addition of 10% AA in the CZO precursor solution (CNZO-AA). The other type of CNZO was produced by mixing the CZO solution and adjusting the solution to pH = 9.0 by adding 1 M $NH_{3(aq)}$ in the solution (CNZO-A). All the prepared solutions were then thermally treated by setting a heating rate at 2°C min^{-1} to 400°C to obtain the doped samples.

The doped ZnO samples were obtained and ready for further analysis. The absorption of the produced samples was characterized using a UV–VIS–NIR spectrometer (V-670 JASCO) in the 0.3–2.5 μm wavelength region. The crystal structure of the ZnO samples was measured using an X-ray diffractometer (XRD, Shimadzu Labx XRD-6000), which emits Ni-filtered Cu-Ka radiation with a 0.15418 nm wavelength at 300 W that scans diffraction angles between 20° and 80° in 0.01° steps at a rate of 1° min^{-1}. The surface structures of the deposited films were analysed to investigate the sample morphology using a scanning electron microscope (SEM, Jeol JSM-5600). The energy levels of the prepared samples were analysed using a linear potential scan method. The linear potential scan measurements were performed using an electrochemical analyzer (type 6081C, CH Instruments) with a three-electrode cell system. The sample film was taken as the working electrode and Pt and Ag/AgCl were used as counter and reference electrodes in a 0.1 M KCl solution as the electrolyte for this measurement. The chemical bonds of the ECD films were analysed by X-ray photoelectron spectroscopy (XPS) system (Thermo Fisher Scientific Inc.) with a monochromatic Al Kα source and charge neutralizer. The linear potential scan measurements were carried out by a potential setup range at a scan rate of 100 mV^{-1}. The data of current *vs.* potential were collected and analysed to evaluate the energy bands for the samples [8].

3. Results and discussion

3.1 *Characterization of N-doped ZnO*

Nitrogen additives, namely ammonia (A), and ammonium acetate (AA), were added in the precursor solutions to prepare the N-doped ZnO (NZO) samples. The crystal

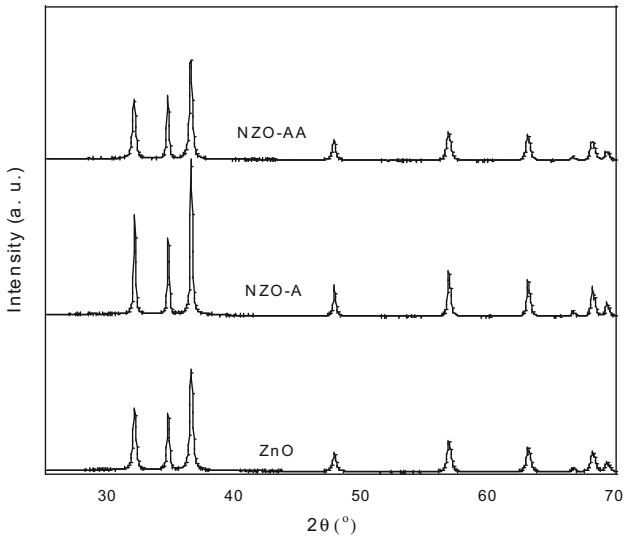

Figure 1. XRD patterns for the N-doped ZnO (NZO) samples.

structure of the prepared samples treated at 400°C was characterized through XRD analysis. Figure 1 illustrates the XRD patterns for the NZO samples. The main peaks in the XRD patterns were observed at 31.7° (100), 34.4° (002) and 36.2° (101), which belong to the hexagonal crystal of ZnO according to the Joint Committee on Powder Diffraction Standards (JCPDS No. 89-0510) database. The annealed crystal ZnO samples, which were originally synthesized in base solution (pH > 8), were reported in literature [8,31]. In figure 1, small-angle variations for the samples were observed in the XRD peaks (i.e., 36.5°). The angle shift implied that the ZnO crystal structure varied because of the N-element additives in ZnO.

The crystallinity of the samples was evaluated using XRD data and the Scherrer equation. The average crystalline sizes of the samples were estimated between 32 nm (ZnO) and 46 nm (NZO-A), as listed in table 1. The size of NZO-A was the largest among all the samples, because the XRD peaks of NZO-A exhibited the sharpest, as shown in figure 1. This implies that ZnO crystals grew the largest size in ammonia solution probably because ZnO crystals formed in basic solution at low temperature and enlarged at 400°C during annealing process.

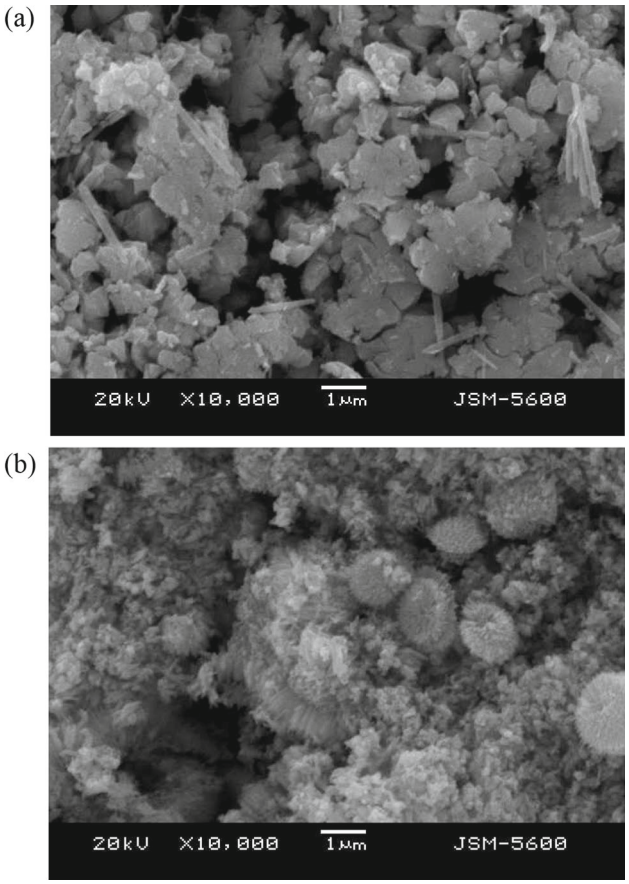

Figure 2. SEM images for (**a**) NZO-A and (**b**) NZO-AA.

The morphologies of the prepared ZnO samples were analysed to demonstrate the influence of the additives on the shape of the ZnO particle. Figure 2 depicts the SEM images of NZO, which was produced in various additives after the thermal treatments. Figure 2a illustrates the SEM image of NZO-A in shapes of particles, including cubic, plate and needle-like shapes, for the sample treated at 400°C. The shape of the NZO-AA particles appeared coral-like and porous, as shown in figure 2b. The SEM images indicate that the morphology of the ZnO samples was influenced by the additives. The difference in particle morphologies, and

Table 1. Properties of the prepared ZnO samples.

Sample	Grain size (nm)	Bandgap (E_g) (eV)	Valence band (E_v) (eV)	Conduction band (E_c) (eV)
ZnO	32	3.15	2.77	–0.38
NZO-A	46	2.98	2.60	–0.38
NZO-AA	32	3.08	2.74	–0.34
CZO	37	3.10	2.81	–0.29
CNZO-A	42	3.00	2.79	–0.23
CNZO-AA	38	3.08	2.88	–0.20

A: Ammonia; AA: ammonium acetate.

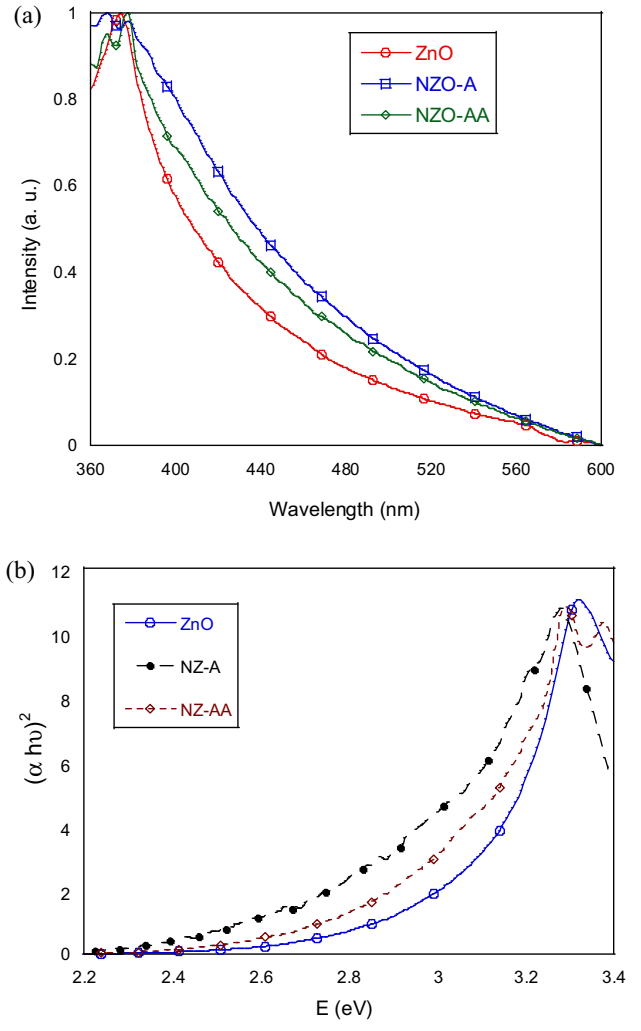

Figure 3. Plots of (**a**) UV–vis spectra and (**b**) $(\alpha h\upsilon)^{1/2}$ *vs.* photonic energy (τ-plot) for the NZO samples.

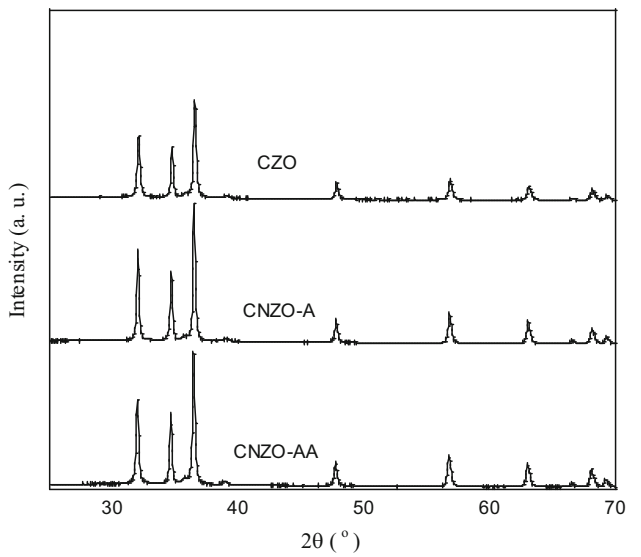

Figure 4. XRD patterns for the Cu- and N-doped ZnO samples.

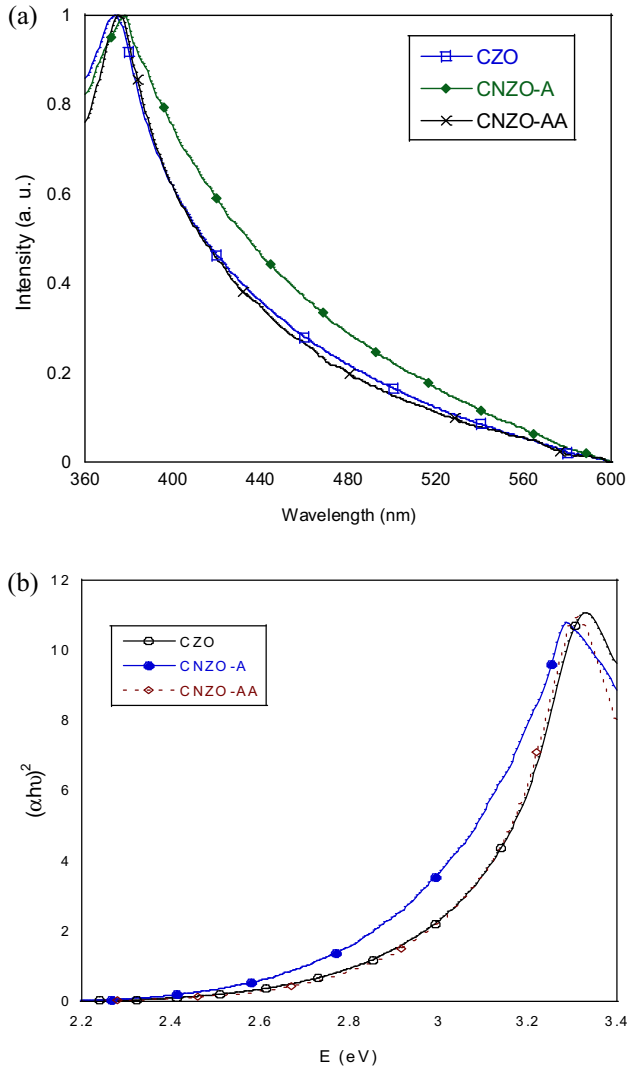

Figure 5. Plots of (**a**) UV–vis spectra and (**b**) $(\alpha h\upsilon)^{1/2}$ *vs.* photonic energy (τ-plot) for the Cu- and N-doped ZnO samples.

grain sizes of these NZO samples were attributed to the presence of the additives during the formation of ZnO.

The light absorption of the NZO samples was revealed through the UV–vis spectra, as shown in figure 3. Figure 3a exhibits the absorption spectra of different NZO samples treated at 400°C. The peak position at 374 nm belongs to the absorption of ZnO. For the NZO samples, the peak positions moved to 377 nm (NZO-AA) and 379 nm (NZO-A), respectively. Additionally, the absorption patterns of NZO-A and NZO-AA between 400 and 600 nm are different from that of ZnO. The results of the spectra analysis indicated a red shift and different light absorption patterns in the visible region. The results suggested that the addition of the additives, such as ammonia, could be a possible approach to modify optical property of ZnO after the thermal treatment.

The photonic bandgap energy (E_g) of the NZO samples can be determined using the UV–vis spectral data. The spectral data were transformed to τ-plot curves, as shown in

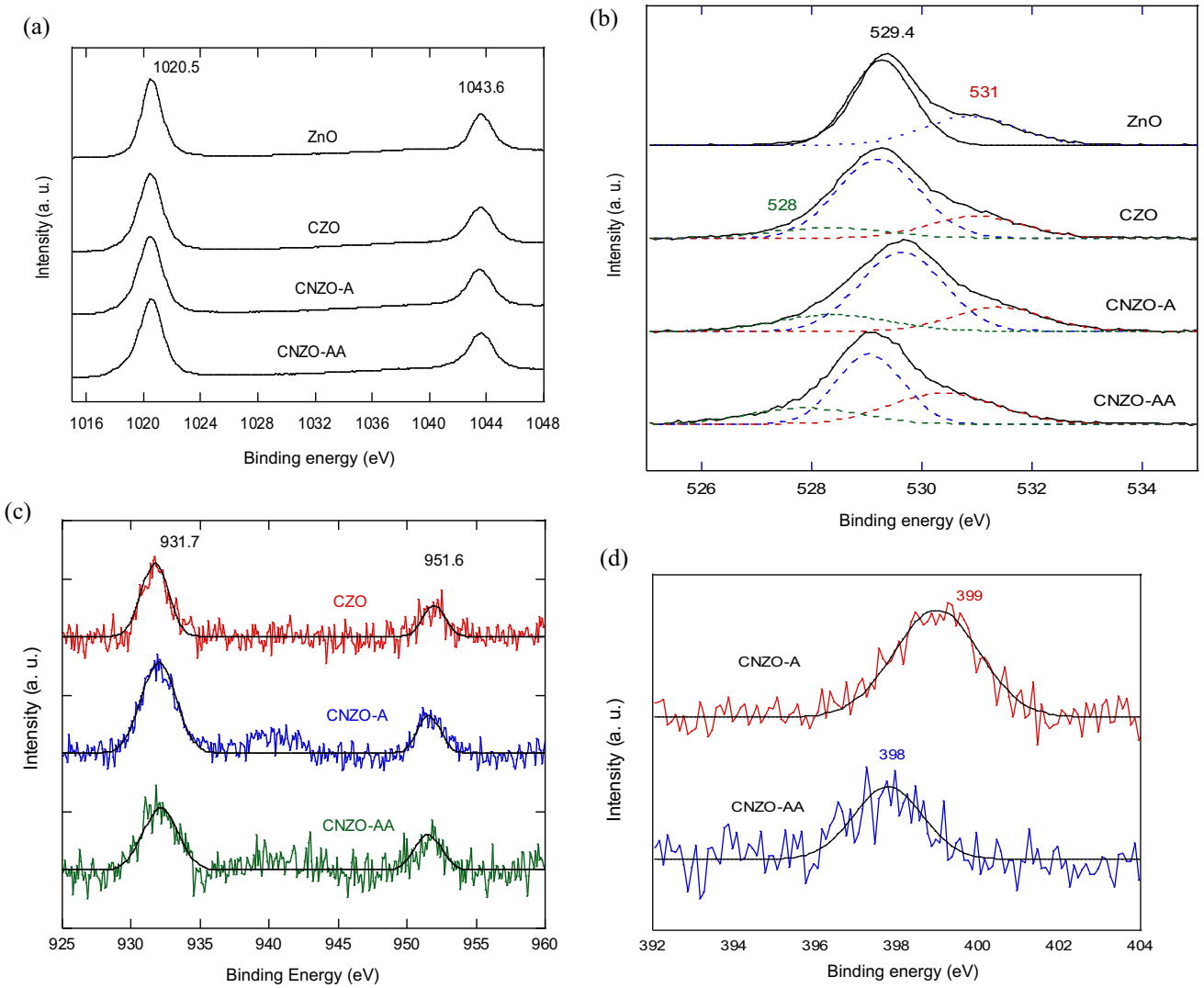

Figure 6. Core-level spectra of (**a**) Zn 2p, (**b**) O 1s, (**c**) Cu 2p and (**d**) N 1s for the doped ZnO samples by XPS survey.

figure 3b. The E_g of the produced ZnO sample without any additives was determined at 3.15 eV. The E_g of the NZO samples was estimated between 2.98 and 3.12 eV, as listed in table 1. This implied that the light absorption of the N-doped ZnO sample was not much affected by this type of the N-source additives. The lowest E_g of NZO occurred for NZO-A probably because the optical property of the ZnO crystals were modified and influenced by the presence of N species in ammonia. The N-containing species in the additives affected the formation of N-doped ZnO on the crystal structure to vary the E_g value. Variations in E_g between ZnO and NZO implied that this recipe of producing ZnO was an influential factor to alter the optical property of ZnO.

3.2 *Characterization of Cu and N co-doped ZnO*

The crystal structure of the prepared CNZO samples treated at 400°C was characterized through XRD analysis, as shown in figure 4. The main peaks in the XRD patterns were observed at 31.7° (100), 34.4° (002) and 36.2° (101), which belong to the hexagonal crystal of ZnO. The average crystalline sizes of the samples were estimated between 38 nm (CNZO-AA) and 42 nm (CNZO-A), as listed in table 1. Variations of the crystal properties for the samples were observed because of the influence of the different recipes on CNZO fabrication during thermal processing.

The Cu-doped ZnO (CZO) sample, without N-element sources, was prepared by adding 5 mol% Cu^{2+} into a Zn^{2+} solution and heating to 400°C. CZO was prepared to evaluate the influence of the presence of Cu on the property of CZO. The average crystalline size of CZO was determined at 37 nm, which is larger than that of ZnO (32 nm). The UV–vis spectrum of the CZO sample is displayed in figure 5a. The peak for CZO was found at 374 nm. The E_g value of CZO was estimated to be 3.10 eV using a τ-plot curve, as shown in figure 5b. The E_g value was lower than that of ZnO (3.15 eV) probably because of the presence of Cu in ZnO.

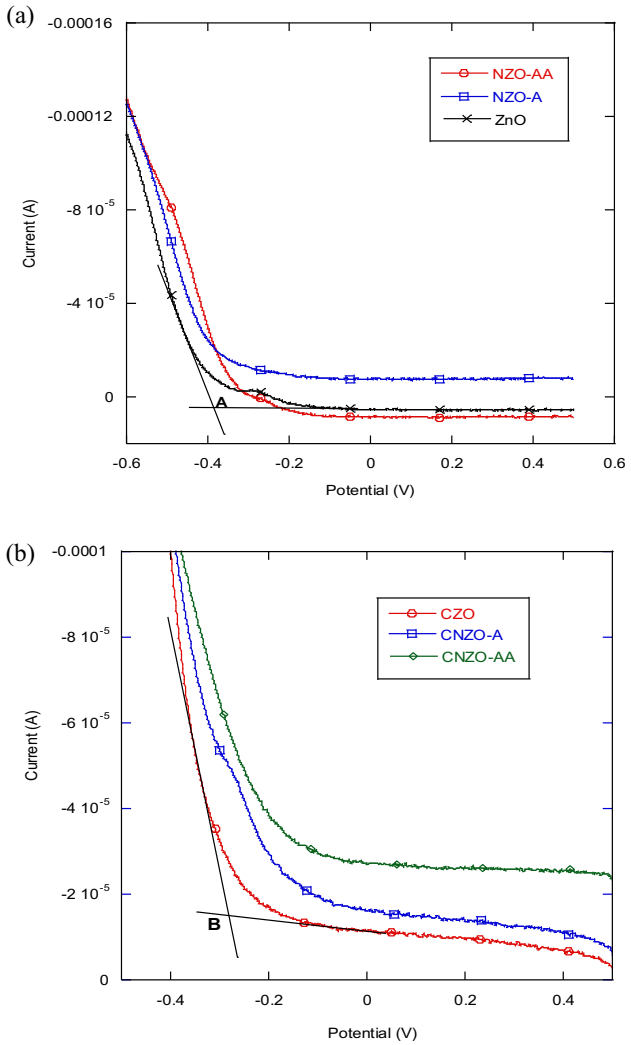

Figure 7. *I–V* curves of linear potential scan in a potential range to determine the E_c values for (**a**) NZO and (**b**) CNZO samples.

The Cu and N co-doped ZnO samples, such as CNZO-A and CNZO-AA, were fabricated by mixing Zn^{2+} with Cu^{2+} and various N additives. The light absorption spectra of these samples are illustrated in figure 5a. The peak positions for the CNZO samples were found at 376 nm (CNZO-AA) and 378 nm (CNZO-A). The peaks moved from 374 nm (ZnO) to a longer wavelength, which indicate a red shift for the CNZO samples. The E_g values of the CNZO samples were 3.0 and 3.08 for CNZO-A and CNZO-AA, respectively, evaluated using the τ-plot (figure 5b). The E_g data of the CNZO samples were lower than those of ZnO (3.15 eV) and CZO (3.10 eV). The lower E_g value implied that the energy band of ZnO was altered by the presence of both Cu and N co-doping in ZnO.

The chemical state of the doped ZnO samples were analysed using XPS measurements. Figure 6 displays the spectra of the binding energies for the elements of the samples. Figure 6a shows the chemical state of Zn in the CNZO samples in the energy range. The significant peaks for Zn element of the samples were shown at 1020.5 and 1043.6 eV, which were assigned to Zn $2p_{3/2}$ and Zn $2p_{1/2}$, respectively [26]. The spectra of O 1s for these ZnO samples were detected, as shown in figure 6b. An asymmetric broad peak for O 1s was observed probably because more than one state of O is present. Two peaks at 529.4 and 531 eV were analysed for the ZnO case, as shown in figure 6b. The peak at 529.4 eV belongs to the binding energy of Zn–O structure, whereas the oxygen defect in ZnO, such as oxygen vacancy, formed and appeared at 531 eV [26,32]. The spectra of Cu for the Cu-containing ZnO samples were detected, as shown in figure 6c. The peaks at 931.7 and 951.6 eV, which were assigned to Cu $2p_{3/2}$ and Cu $2p_{1/2}$, for Cu in CZO are displayed in figure 6c [33]. Additionally, three peaks in the spectra of Cu-containing ZnO were observed, as shown in figure 6b. The peak at 528 eV for the CZO case appeared because of the presence of a small amount of Cu in ZnO. This suggests that Cu–O structure formed in the CZO case according to the spectral analysis. In the previous analysis, the crystal data (XRD) and E_g analysis of CZO varied from those of ZnO, which implies that Cu was chemically bonded with ZnO.

The chemical state of both Cu- and N-containing ZnO (CNZO) samples were further analysed by XPS data. The chemical states of Cu and Zn species for CNZO are Zn–O and Cu–O, according to the XPS spectral analysis using the data in figure 6a–c. Furthermore, the spectra of N 1s for CNZO were detected as shown in figure 6d. The intensities of the XPS spectra for N 1s in the CNZO samples were weak, which means a very small amount of N species was detected in CNZO. Among the cases, CNZO-A exhibited the most significant intensity of N species in the CNZO samples. The peaks for the CNZO samples were shown at 399 (CNZO-A) and 398 eV (CNZO-AA). The variation of the peak location indicated that N in CNZO, which was fabricated using different N additives, formed various chemical structures in the samples. The peak at 399 eV was assigned to N bonded with Zn (O–Zn–N), whereas the peaks at lower energies between 396 and 398 eV were corresponding to several possible chemical structures, such as N–Zn–N, N–C and N–H [34]. The presence of various chemical states of N species in CNZO can be one of the influential factors to alter the sample property, such as E_g (optical absorption).

3.3 *Energy-level variation for doped ZnO*

The energy band levels of the prepared samples were evaluated to study the influence of the presence of Cu and N on the ZnO samples. The energy levels for the doped ZnO samples, including the conduction band minimum (E_c) and valence band maximum (E_v), were determined using both linear potential scan measurements and UV–vis spectral data. Figure 7 depicts the current–potential curves in the potential range between +0.5 and –1.0 V for the samples.

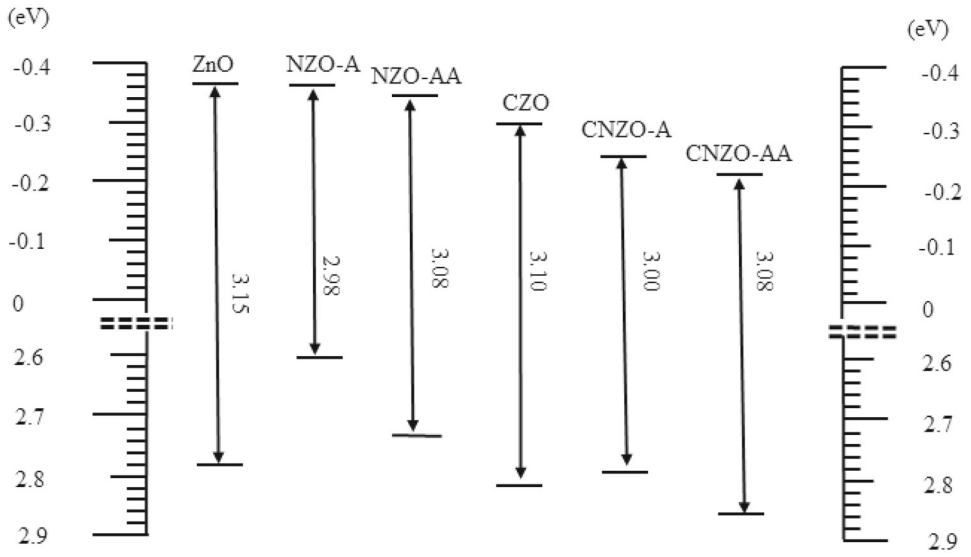

Figure 8. Energy band diagram for various Cu and N doping in ZnO samples.

The current significantly increased after –0.3 V for the ZnO and N-doped ZnO samples and –0.2 V for the Cu-doped and Cu and N co-doped ZnO samples, as shown in figure 7a and b. The E_c values of the samples corresponding to the increase in the current were estimated according to the current–potential curves. The E_c values of ZnO and CZO at intersection of the two slopes at points A and B were –0.38 and –0.29 eV, respectively, in the current–potential curves, as shown in figure 7. After the E_c values of the samples were obtained, the E_v values can be evaluated using the E_g value, which is the difference between the E_c and E_v values and determined through the previous UV–vis spectral analysis as listed in table 1. Hence, the influence of the presence of N and Cu in ZnO crystals on the energy bands was evaluated when the energy levels were determined.

The energy levels of the modified ZnO samples are plotted in figure 8. With ZnO as reference, the E_c values of N-doped ZnO, such as NZO-A and NZO-AA, were the same as that of ZnO. This implied that the presence of N in ZnO crystals did not affect the E_c distribution. However, the E_v of N-doped ZnO was lower than that of ZnO in the presence of N in the crystal. The E_g of N-doped ZnO decreased because of the variation in E_v, as shown in the band diagram (figure 8). Both E_c and E_v for Cu-doped ZnO (CZO) were 0.05 and 0.04 eV, different from those of ZnO, respectively. This indicated that the presence of Cu in ZnO changed both energy levels, which reduced the E_g value of ZnO. From the energy-level analysis, either N (nonmetal) or Cu (metal) in ZnO revealed different energy-level variations.

The energy levels of E_c and E_v values considerably varied for the Cu and N co-doped ZnO (CNZO) samples, according to the band distribution in figure 8. The E_c values of CNZO were approximately 0.15 eV lower than that of ZnO, whereas the E_v values were all higher than that of ZnO, as shown in table 1. In the previous analysis, the difference of E_c between CZO and ZnO was 0.05 eV, which was mainly caused by Cu instead of N in ZnO. However, the variation in E_c was 0.07 eV lower for CNZO than for CZO because of the presence of both Cu and N. Similarly, although the E_v values of NZO were lower than that of ZnO, the E_v values of CNZO were larger than that of ZnO. The variation in the energy bands of the CNZO samples was caused by the presence of both Cu and N with ZnO. This suggested that the interaction of Cu and N with ZnO could probably result in considerably lower E_c and larger E_v values. From the XPS analysis, various compositions of Cu/N in ZnO were analysed and attributed to different fabrication recipes for producing CNZO. The degree of energy-level variations among the CNZO samples can be corresponding to its chemical composition of Cu and N in ZnO crystals.

4. Conclusions

Various types of doped ZnO crystals, including NZO, CZO and CNZO, were fabricated and characterized. The morphology and crystalline size of the doped ZnO varied in the presence of different dopants. The energy bands for all the ZnO-doped samples were determined and varied because of the presence of the dopants from linear sweep voltammetry and UV–vis data analysis. The E_g values of the doped ZnO samples decreased in the presence of Cu and N, which caused the red shift of light absorption. The E_c value for NZO maintained the same, whereas the E_v was lower than that of ZnO in the presence of N in ZnO crystal. However, both E_c and E_v distribution for CNZO considerably varied in the presence of Cu and N in ZnO. The degree of energy-level variations among the CNZO samples can be

corresponding to its chemical composition of Cu and N in ZnO crystals, according to the XPS spectral analysis.

Acknowledgement

This study is partially supported by the Ministry of Science and Technology, Taiwan, under grant MOST108-2221-E-155-026. The financial support is gratefully acknowledged.

References

[1] Qi K, Cheng B, Yu J and Ho W 2017 *J. Alloys Compd.* **727** 792
[2] Ong C B, Ng L Y and Mohammad A W 2018 *Renew. Sust. Energ. Rev.* **81** 536
[3] Samadi M, Zirak M, Naseri A, Khorashadizade E and Moshfegh A Z 2016 *Thin Solid Films* **605** 2
[4] Yang X, Wolcott A, Wang G, Sobo A, Fitzmorris R C, Qian F *et al* 2009 *Nano Lett.* **9** 2331
[5] Park J S, Kim H and Kim I D 2014 *J. Electroceram.* **32** 117
[6] Sharma P K, Kumar M and Pandey A C 2011 *J. Nanopart. Res.* **13** 1629
[7] Nomura K, Ohta H, Takagi A, Kamiya T, Hirano M and Hosono H 2004 *Nature* **432** 488
[8] Liau L C-K and Huang J S 2017 *J. Alloys Compd.* **702** 153
[9] Fu M, Li Y, Wu S, Lu P, Liu J and Dong F 2011 *Appl. Surf. Sci.* **258** 1587
[10] Lee W J, Kang J and Chang K J 2006 *Phys. Rev. B* **73** 024117
[11] Xie X Y, Zhan P, Li LY, Zhou D J, Guo D Y, Meng J X *et al* 2015 *J. Alloys Compd.* **644** 383
[12] Kani Amuthan B, Vinoth S, Karthikeyan V, Roy V A L and Thilakan P 2019 *Ceram. Int.* **45** 24324
[13] Kumari R, Sahai A and Goswami N 2015 *Prog. Nat. Sci.: Mater. Int.* **25** 300
[14] Qin H, Li W, Xia Y and He T 2011 *ACS Appl. Mater.* **3** 3152
[15] Kumar S, Baruah A, Tonda S, Kumar B, Shanker V and Sreedhar B R 2014 *Nanoscale* **6** 4830
[16] Bhirud A P, Sathaye S D, Waichal R P, Nikam L K and Kale B B 2012 *Green Chem.* **14** 2790
[17] Peter C N, Anku W W, Sharma R, Joshi G M, Shukla S K and Govender P P 2019 *Ionics* **25** 327
[18] Oliveira J A, Nogueira A E, Gonçalves M C P, Paris E C, Ribeiro C, Poirier G Y *et al* 2018 *Appl. Surf. Sci.* **433** 879
[19] Gionco C, Fabbri D, Calza P and Paganini M C 2016 *J. Nanomater.* **2016** 4129864
[20] Wang J D, Liu J K, Tong Q, Lu Y and Yang X H 2014 *Ind. Eng. Chem. Res.* **53** 2229
[21] Prabakaran E and Pillay K 2019 *RSC Adv.* **9** 7509
[22] Sun S, Chang X, Li X and Li Z 2013 *Ceram. Int.* **39** 5197
[23] Sharma S, Mehta S K and Kansal S K 2017 *J. Alloys Compd.* **699** 323
[24] Chen Z, Yan Q, Zhao Y, Cao M, Wang J and Wang L 2019 *J. Sol-Gel Sci. Technol.* **91** 101
[25] Qiu Y, Yan K, Deng H and Yang S 2012 *Nano Lett.* **12** 407
[26] Wang M, Ren F, Zhou J, Cai G, Cai L, Hu Y *et al* 2015 *Sci. Rep.* **5** 12925
[27] Hou S and Li C 2016 *Thin Solid Films* **605** 37
[28] Shet S, Ahn K S, Deutsch T, Wang H, Nuggehalli R, Yan Y *et al* 2010 *J. Power Sources* **195** 5801
[29] Lu J G, Ye Z Z, Zhuge F, Zeng Y J, Zhao B H and Zhu L P 2004 *Appl. Phys. Lett.* **85** 3134
[30] Patel P P, Hanumantha P J, Velikokhatnyi O I, Datta M K, Hong D, Gattu B *et al* 2015 *J. Power Sources* **299** 11
[31] Goswami N and Sharma D K 2010 *Physica E* **42** 1675
[32] Yao Z, Tang K, Xu Z, Ye J, Zhu S and Gu S 2016 *Nanoscale Res. Lett.* **11** 511
[33] Sankar Ganesh R, Durgadevi E, Navaneethan M, Patil V L, Ponnusamy S, Muthamizhchelvan C *et al* 2018 *Sens. Actuator A Phys.* **269** 331
[34] Muthulingam S, Bae K B, Khan R, Lee I and Uthirakumar P 2015 *RSC Adv.* **5** 46247